



Effect of PEDOT:PSS Layer Deposition on Electrical and Photoelectrical Properties of n^+ -ZnO/ n -Si Heterostructure

Y. V. Gomeniuk¹ · Y. Y. Gomeniuk¹ · S. V. Kondratenko² · T. E. Rudenko¹ · A. V. Vasin^{1,3,4} · A. V. Rusavsky¹ · O. M. Slobodian¹ · I. P. Tyagulskyy¹ · V. P. Kostylyov¹ · V. M. Vlasjuk¹ · S. I. Tiagulskiy³ · R. Yatskiv³ · V. S. Lysenko¹ · A. N. Nazarov^{1,4}

Received: 21 October 2022 / Accepted: 24 January 2023 / Published online: 17 February 2023
© The Author(s) 2023

Abstract

The results of electrical and photoelectrical characterization of the interface and bulk properties of n^+ -ZnO/ n -Si and poly(3,4-ethylene dioxythiophene):poly(styrenesulfonate) (PEDOT:PSS)/ n^+ -ZnO/ n -Si heterostructures are presented. It was found that the PEDOT:PSS layer deposited on the surface of zinc oxide increases the potential barrier at the ZnO/Si interface, leading to higher band bending in the silicon, which is important for solar cell applications. The recombination rate at the interface decreases because of the creation of an inversion layer in the silicon under operational conditions. The increase of the potential barrier in PEDOT:PSS/ n^+ -ZnO/ n -Si heterostructures results in the increase of the open-circuit voltage by 54–180%. The external quantum efficiency in PEDOT:PSS/ n^+ -ZnO/ n -Si heterostructures increases by 100% at 450 nm.

Keywords ZnO thin films · solar cells · organic–inorganic heterojunctions · impedance spectroscopy · interface traps

Introduction

Both inorganic transparent zinc oxide (ZnO) and organic conducting polymer poly(3,4-ethylene dioxythiophene):poly(styrenesulfonate) (PEDOT:PSS) films have recently occupied a wide niche of applications related to photovoltaic cells, which are the key elements of green energetics. Given the intrinsic n -type conductance of ZnO, it was suggested as an electron-collecting layer,^{1–3} replacing the expensive indium tin oxide (ITO); intrinsically p -type PEDOT:PSS is often used as a hole-collecting layer in perovskite⁴ and

hybrid organic silicon heterojunction solar cells.^{5–8} Several more exotic applications of PEDOT:PSS/ZnO structures have also been reported, such as resistive switching devices,⁹ optoelectronic sensors,¹⁰ liquified petroleum gas sensors,¹¹ and ultraviolet light-emitting diodes.¹² A heterojunction consisting of a PEDOT:PSS layer deposited on ZnO nanorods synthesized at the surface of n -type silicon has been suggested as a simple, non-toxic, and low-cost UV light photodetector.¹³

Understanding the electronic properties of the PEDOT/ZnO and ZnO/Si interfaces is of great importance in further development of relevant heterostructures for photovoltaic and optoelectronic applications. It has been reported that deposition of p -type PEDOT:PSS onto n -type ZnO enables one to improve the reliability of ZnO, preventing the adsorption and desorption of oxygen molecules on the ZnO crystal surface.¹⁴ In that paper, non-intentionally doped single-crystalline ZnO was studied, and it was shown that the charge transport between the PEDOT:PSS and bulk ZnO depends on the polarity of the crystal surface.

In the present work we have used highly doped n^+ -ZnO films deposited by magnetron sputtering on n -type silicon. The doping of ZnO films was performed by adding methane during the deposition process. Recently, it has been demonstrated that methane can be effectively used for deposition

✉ Y. V. Gomeniuk
yurigom@workmail.com

¹ Lashkaryov Institute of Semiconductor Physics, National Academy of Sciences of Ukraine, 41 Pr. Nauki, Kyiv 03028, Ukraine

² Taras Shevchenko National University of Kyiv, 64 Volodymyrs'ka St, Kyiv 01601, Ukraine

³ Institute of Photonics and Electronics, Czech Academy of Sciences, Chaberská 1014/57, 18251 Prague, Czech Republic

⁴ National Technical University of Ukraine “Igor Sikorsky Kyiv Polytechnic Institute”, 37 Pr. Peremohy, Kyiv 03056, Ukraine

of conductive ZnO films.^{15,16} The electrical and photoelectrical properties of both ZnO/*n*-Si heterostructures and hybrid PEDOT:PSS/ZnO/*n*-Si heterostructures were studied. Capacitance–voltage (*C–V*) and current–voltage (*I–V*) measurements and impedance spectroscopy were applied to investigate the effect of PEDOT:PSS deposition on the potential barriers, the density of surface states, and the recombination lifetime at the ZnO/Si interface. The spectral dependences of the external quantum efficiency (EQE) were measured to understand the effect of PEDOT:PSS on the photovoltaic properties of the ZnO/Si heterostructure.

Samples and Experimental

Sample Preparation

Zinc oxide films were deposited on *n*-type silicon wafers (5 ohm × cm) and glass slides by RF (13.56 MHz) magnetron sputtering. The deposition was carried out in an argon/methane gas mixture at a working pressure of 10⁻¹ Pa. The ratio of Ar/CH₄ during deposition was kept at 4:1. Further details of the deposition process can be found in Refs. 15,16 The thicknesses of the deposited zinc oxide film were 75 nm and 135 nm. For the electrical measurements, circular Ni dots (1.2 mm diameter) were deposited onto the ZnO surface by DC magnetron sputtering. The second contact was formed by rubbing Ga/Zn eutectic into the back side of the silicon wafer. This procedure was applied to prepare the Ni/ZnO/*n*-Si heterostructures. For electrical testing of the ZnO layers, several samples of ZnO/glass structures were fabricated in the same as the ZnO deposition.

A hybrid PEDOT:PSS/ZnO/Si heterostructure was formed by PEDOT:PSS solution spin-coating onto the surface of the ZnO film at 3000 rpm for 20 s, followed by thermal annealing at 140°C for 30 min under standard atmospheric conditions. Finally, a gold electrode (circular dot of 1.5 mm diameter) was thermally evaporated on the polymer surface as a top contact and a Ga/Zn eutectic was scratched into the *n*-type silicon as a back contact.

The choice of metal contact for each type of heterostructure was made taking into account the closeness of the metal workfunction to the position of the Fermi energy for PEDOT:PSS or ZnO to provide a good non-rectifying contact between the metal and the film.

Characterizations

The metal–semiconductor and metal–organic–semiconductor heterojunctions were characterized by *C–V*, conductance–frequency (*G–ω*) and *I–V* measurements with an Agilent 4284 LCR meter and a Keithley 6485 picoammeter. Resistivity and Hall mobility were measured using Van der

Paw and Hall effect methods by the ezHEMS Hall effect measurement system (NanoMagnetics Instruments, UK).

Spectral and photoelectric measurements were carried out using the following equipment and standard samples: solar simulator; reference photovoltaic cells; set-up for photoelectrical parameters tests of solar cells; set-up for measuring of the spectral characteristics of photoconverters; and software to automate testing.

The spectral dependences of the external quantum efficiency EQE (λ) were measured using the sample's short-circuit mode in the wavelength range $\Delta\lambda$ of 360–1200 nm, with the grating monochromator automatically maintaining constant flux of the monochromatic photons at a specified level. For this, the photon flux was divided, using an oscillating beam splitter with a frequency of 20 Hz, into the channel for maintaining the photon flux at a given constant level, and into the channel for measuring the EQE of the sample under investigation. In this case, the photon flux was modulated with a frequency of 20 Hz. The amplification on an alternating signal with a frequency of 20 Hz, followed by a lock-in amplifier, improved the signal-to-noise ratio (see supplementary Figure S1).

Results and Discussion

Determination of the Potential Barrier in the *n*⁺-ZnO/*n*-Si Interface

Table I demonstrates the results obtained by the Hall effect and Van der Paw measurements on the ZnO films with different thicknesses. The experiment shows that the ZnO films are highly doped *n*-type ones with nearly the same doping concentration of about 1.5 × 10²⁰ cm⁻³. The thicker ZnO film has a higher Hall mobility which can be associated with larger grain sizes in such polycrystalline films (see supplementary Figure S2).

Figure 1a shows the *I–V* dependences for ZnO/Si and PEDOT:PSS/ZnO/Si heterostructures with a 75-nm-thick ZnO layer. The *I–V* characteristics show clear asymmetry reflecting the presence of a potential barrier inside the structure. To make sure that this barrier is not due to a possible Schottky barrier at the metal contact with ZnO (or PEDOT:PSS) film we measured the *I–V* dependences

Table I Hall mobility and average doping concentration in the ZnO films with different thicknesses deposited in Ar/CH₄ gas mixing

Structure	ZnO thickness, nm	Resistivity, ohm × cm	Hall mobility, cm ² /V × s	Concentration, cm ⁻³
ZnO/glass	135	4.5 × 10 ⁻³	8.5	1.6 × 10 ²⁰
ZnO/glass	75	6.6 × 10 ⁻³	6.2	1.5 × 10 ²⁰

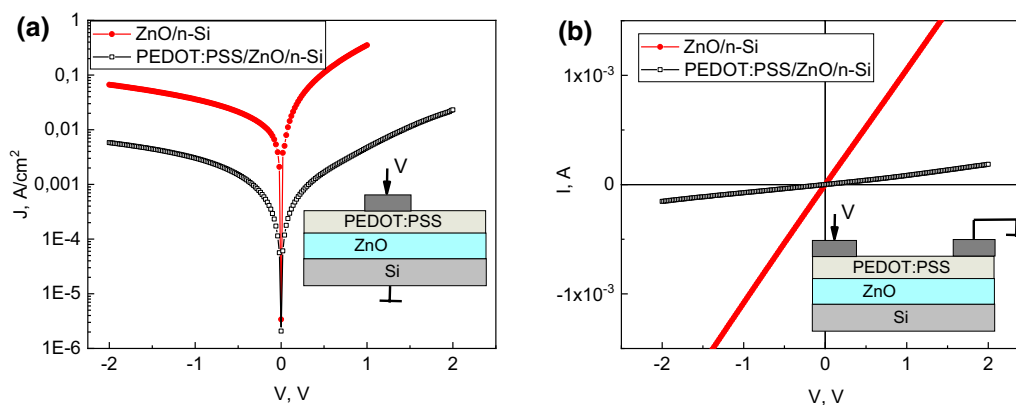


Fig. 1 (a) Current–voltage characteristics for ZnO/n-Si (red) and PEDOT:PSS/ZnO/n-Si (black) heterostructures. (b) I – V curves measured in co-planar geometry on ZnO (red) and PEDOT:PSS (black).

Insets the scheme of respective measurements for the PEDOT:PSS/ZnO/n-Si structure; for the ZnO/n-Si structure, the metal contacts lie on the ZnO layer (Color figure online).

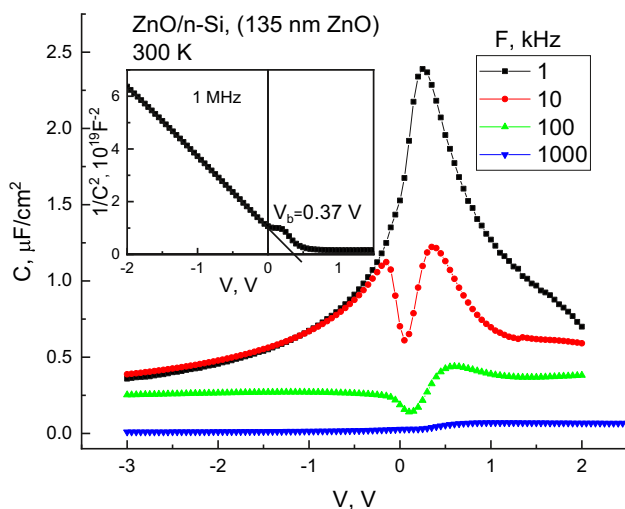


Fig. 2 Capacitance–voltage characteristics for the Ni/ZnO/n-Si heterostructure at four different frequencies. Inset the Mott-Schottky plot for the determination of the built-in voltage (Color figure online).

in co-planar geometry between two contacts on the top of the ZnO or PEDOT:PSS films, and the respective curves are shown in Fig. 1b. They show an ideally linear behavior, which confirms that the potential barrier at the metal–film interface is absent or negligibly small, although the absolute value of the resistance is much higher in the case of PEDOT:PSS film. We attribute this to the poor contact resistance between the metal and the PEDOT:PSS layer, which also leads to much lower currents being measured across the sample for the PEDOT:PSS/ZnO/Si heterostructures (see Fig. 1a).

Figure 2 shows the C – V dependences for the ZnO/Si heterostructure with a 135-nm-thick ZnO layer measured at four different frequencies. We should note that a typical

decrease of total capacitance towards negative bias, which reflects the widening of the depletion layer in silicon, is observed, either at low (1 kHz) or high (1 MHz) measurement frequencies. The absolute value of capacitance at negative bias drops by approximately an order of magnitude with the increase of frequency from 1 kHz to 1 MHz. The possible reason for this is that, at high frequencies and at depletion (negative) bias, a large portion of the ZnO film is rather more dielectric than a conductor because the lack of free carriers, and the capacitance of the depleted ZnO layer becomes connected in series to the capacitance of the rest of the structure. At low frequencies, minority carriers are able to follow an ac testing signal,¹⁷ and the ZnO layer effectively behaves as a conductor. At intermediate frequency (100 kHz), due to the capacitive response from recharging of interface traps, capacitance behavior becomes more complicated, so we cannot observe the characteristic depletion tail in the C – V plot (see Fig. 2, green curve).

Following a Mott-Schottky approach, the intercept of $1/C^2$ versus V plot with the x -axis gives the built-in voltage, V_{bi} , at the silicon–zinc oxide interface. The barrier height, ϕ_b , is connected with the built-in voltage, V_{bi} , (or band bending, in other words) with the equation¹⁸:

$$\phi_b = V_{bi} + (E_C - E_F) + \frac{kT}{q} \quad (1)$$

where E_C is the energy of the bottom of the conduction band, E_F is the Fermi energy in silicon, k is the Boltzmann constant, and T is the absolute temperature.

The Mott-Schottky plot for the Ni/ZnO/Si heterostructure is shown in the inset in Fig. 1. Here, the results are presented for the C – V curve measured at 1 MHz, when the contribution of interface traps can be neglected.

For an ideal case, taking into account a high doping level of zinc oxide, the donor concentration of 10^{15} cm^{-3} in silicon and the intrinsic conduction band offset of 0.4 eV (due to the difference in electron affinity), at 300 K there should be a small built-in voltage of 0.14 V at the ZnO/Si interface. We derived the built-in voltages of 0.37 eV for 135-nm-thick ZnO and 0.34 eV for 75-nm-thick film from the $C-V$ measurements. These values are higher than the expected theoretical ones, which means that, in our case, there exists some density of a fixed negative charge in the interface native oxide layer between ZnO and silicon, which increases the barrier height. This is also one of the reasons why we could not obtain a good barrier for the ZnO/ p -Si system, because the fixed negative charge induces accumulation in the near-surface layer instead of the expected depletion.

In PEDOT:PSS/ZnO/Si heterostructures, the measured V_{bi} was 0.87 eV for 135-nm ZnO and 0.77 eV for 75-nm ZnO, i.e., the organic layer deposited on top of the ZnO film was found to increase the band bending at the ZnO/Si interface. This can be understood if we assume that, after the contact between the p -type polymer and the n -type semiconductor, the charge redistribution occurs as in a conventional $p-n$ junction, leading to the formation of a depleted layer and the appearance of an additional potential barrier. In Ref. 19 various inorganic/organic hybrid heterojunctions were studied as conventional diodes, and it was shown that, for the ZnO/PEDOT:PSS heterostructure, the resulting barrier equals 0.398 eV. This value is very close to the difference between barriers with and without PEDOT:PSS.

Formation of the potential barrier after deposition of the organic polymer onto the ZnO/Si heterostructure is shown in Fig. 3, where the band diagrams are presented for the PEDOT:PSS/ZnO/ n -Si (a) and ZnO/ n -Si (b) heterostructures. These diagrams are plotted based on the work function values and band gap widths for PEDOT:PSS and ZnO reported in Refs. 9,20,21. The key question for the PEDOT:PSS/ZnO/ n -Si structure is whether the electric field penetrates through the ZnO layer or it is screened due to free carriers, as can be expected for the high electron concentration obtained from Hall measurements. To check the uniformity of the current flow through the ZnO layer, we have carried out scanning spreading resistance microscopy (SSRM) measurements, which give information about the spatial distribution of the current through the film over the film surface. The SSRM revealed a strong inhomogeneity of the current flow, so that points with low resistance are separated by large areas with much higher (up to three orders of magnitude) resistance (see supplementary Figure S3). This allowed us to draw the band diagram shown in Fig. 3a, and to suggest that, from the capacitance measurements, we get the information about band bending and space charge region width in silicon, and about the recharging of electrically active centers in the ZnO/Si interface. The ZnO

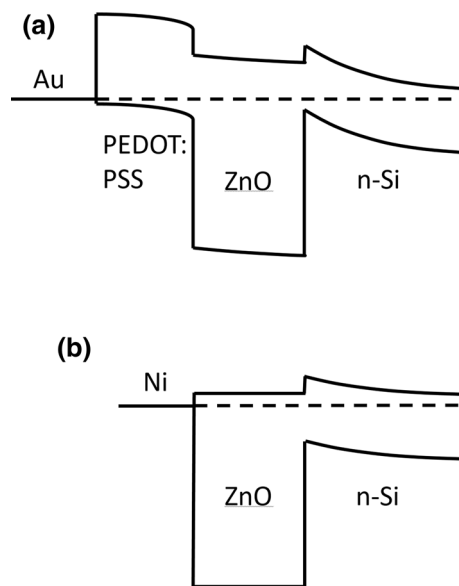


Fig. 3 Band diagrams for the Au/PEDOT:PSS/ZnO/ n -Si heterostructure (a) and the Ni/ZnO/ n -Si heterostructure (b) at zero applied voltage.

film in the PEDOT:PSS/ZnO/ n -Si heterostructure appears to be depleted of charge carriers, which also results in its much higher resistivity than in the case of the ZnO/ n -Si heterostructure.

The barrier height, ϕ_b , at the heterointerface can also be estimated from the $I-V$ characteristics. For extraction of such parameters of the heterojunctions as barrier height, ideality factor, n , and series resistance, R_S , we have used the technique of Cheung and Cheung²² based on the thermionic emission model of current flow. According to their approach, the forward branch of the $I-V$ characteristic obeys:

$$\frac{dV}{d(\ln I)} = IR_S + \frac{nkT}{q} \tag{2}$$

where R_S is the series resistance, n is the ideality factor, k is the Boltzmann constant, T is the absolute temperature, and q is the elementary charge. The dependence $\frac{dV}{d(\ln I)}$ versus I is a straight line, the slope of which gives the series resistance, and the intercept with the y -axis gives the ideality factor. The ideality factor value can then be used for evaluation of the barrier height, ϕ_b , from:

$$V - \frac{nkT}{q} \ln\left(\frac{I}{AA^*T^2}\right) = n\phi_b + IR_S \tag{3}$$

where A is the area of the diode and A^* is the Richardson constant.

Obtained in such a way, the values of ϕ_b , R_S , and n , together with magnitudes of the built-in voltages, V_{bi} , extracted from the $C-V$ measurements, are presented in

Table II. The difference between the bottom of the conduction band and the Fermi energy ($E_C - E_F$) in silicon with a carrier concentration of 10^{15} cm^{-3} at 300 K equals 0.26 eV. Therefore, for the structures without a PEDOT:PSS layer, we can expect from Eq. 1 slightly (by 0.1 eV) higher barriers, than derived from the I - V characteristics. The lower actual values of φ_b can be explained by potential fluctuations at the ZnO/Si interface, the presence of which is also confirmed by the rather high values of the ideality factor. For the structures with a PEDOT:PSS layer, the barriers extracted from I - V are lower than the band bending calculated from the C - V characteristics. It seems that the thermionic emission model does not correctly describe the current through the heterostructure in this case. The detailed analysis of the current flow in such systems needs more study and is beyond the scope of this paper.

It should also be noted that the thicker ZnO film (135 nm) exhibits a much lower value of the ideality factor, reflecting a higher quality of the interface. This can be explained by the fact that, during the ZnO film growth, the film is subjected to hydrogen doping, and the longer this process, the longer the time during which the interface is subjected to hydrogen, which effectively diffuses to the interface and anneals the interface defects, improving the interface quality. The series resistance is also lower for the thicker ZnO film due to the higher carrier concentration and mobility (see Table I). Deposition of a PEDOT:PSS layer on top of the ZnO film results in the dramatic increase of R_S because of depletion of the ZnO layer, as discussed above.

Determination of Interface State Density

The interface state density at the ZnO/Si interface was determined from the G - ω measurements using the classical approach of Nicollian and Goetzberger.^{23,24} This technique is commonly used to study the electrically active states at the interface between the dielectric and the semiconductor. However, this method was primarily developed for SiO_2/Si systems with negligible leakage currents. In the case of leaky dielectric layers or heterostructures, the G - F curves needs in correction, as described in Refs. 25,26. Before the conductance related to interface traps is plotted in G/ω versus frequency coordinates, the parasitic dc conductance

should be subtracted from the measured value. The value of the dc conductance, G_{DC} , is determined by differentiating the current-voltage dependences.

Figure 4 shows the dependences of $(G-G_{DC})/\omega$ versus frequency for the Ni/ZnO/Si heterostructure measured at 300 K with different voltages applied to the top metal electrode. From the maximum value of the G/ω versus the frequency curve, the density of interface states, D_{it} , is determined using the equation $D_{it} = 2.5(G/\omega)_{\max}/(qA)$, where q is the electron charge and A is the sample area.²⁴ It can be seen that, at negative gate voltages, corresponding to depletion of the silicon surface layer, the maximum value is lower than at positive gate voltages, corresponding to the accumulation of the silicon surface by majority carriers. With the change in the gate voltage from positive to negative values, the energy position, at which a Fermi level crosses the ZnO/Si interface, is shifted from the edge of the band gap towards its center. The frequency, at which the maximum of G/ω is observed, changes when the gate voltage is swept, reflecting different characteristic time constants of recharging for interface traps situated at different energy levels within the silicon band gap.

It is evident that, at zero applied voltage, the Fermi level crosses the ZnO/Si interface in the upper half of the

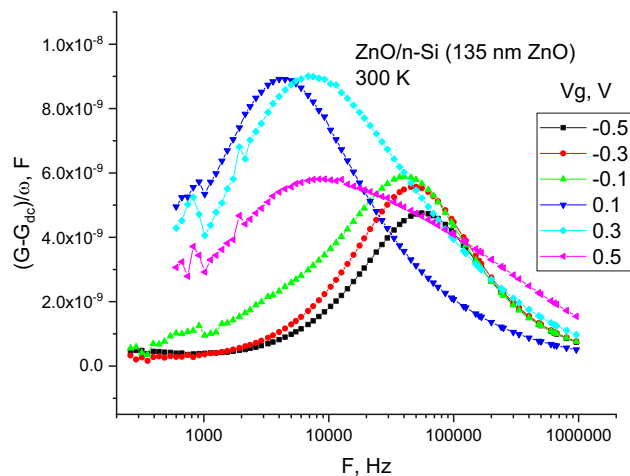


Fig. 4 Dependences of conductance on frequency at different gate biases (step 0.2 V) for the Ni/ZnO/n-Si heterostructure.

Table II Open-circuit voltage V_{OC} , short-circuit current I_{SC} , built-in voltage V_b , barrier height φ_b , series resistance R_S , and ideality factor n

Heterostructure	ZnO thickness, nm	V_{OC} , V	I_{SC} , μA	V_{bi} , V (C - V)	φ_b , V (I - V)	R_S , Ω	n
ZnO/n-Si	135	0.13	860	0.37	0.53	40	4.2
ZnO/n-Si	75	0.125	450	0.34	0.51	48	10.9
PEDOT:PSS/ZnO/n-Si	135	0.2	54	0.87	0.60	2630	7.8
PEDOT:PSS/ZnO/n-Si	75	0.35	60	0.77	0.62	3503	13.5

silicon band gap for the structure without a PEDOT:PSS layer (Fig. 3b), and in the lower half of the band gap (in strong inversion at $E_C - E_F \sim 1$ V) for the structure with a PEDOT:PSS layer (Fig. 3a). Figure 5 presents the dependences of interface states density on gate voltage for the Ni/ZnO/n-Si samples with different thicknesses of ZnO (open symbols, left y-axis). When the bias is swept from negative to positive voltages, the cross-point shifts from the midgap to the bottom of the conduction band for the ZnO/n-Si heterostructure. The density of interface states near the midgap is lower than near the conduction band edge, as could be expected.

The dependences of G/ω_{\max} for the samples with a PEDOT:PSS layer are shown in Fig. 5 by solid symbols (right y-axis). However, for the case of strong inversion, these values are not related to the recharging of the states within the band gap, but reflect the process of minority carrier generation in the space charge region of the silicon.²⁴ In this case, the $G-\omega$ measurements allow us to estimate the minority carrier generation time.²⁷

Determination of the Effective Carrier Lifetime in Subsurface Si Layer

The analysis of interface states recharging or carrier recombination processes, which are important for the operation of solar cells, can be carried out using impedance spectroscopy. This is a kind of ac electrical measurement technique when the complex admittance, Z , or complex impedance, Y , of the structure is measured at a given bias as a function of ac testing signal frequency. The dependence of $\text{Im}(Z) = X$ on $\text{Re}(Z) = R$, or the dependence of $\text{Re}(Y)/\omega = G/\omega$ on $\text{Im}(Y)/\omega = C$ are called Nyquist or Cole–Cole plots.^{28–30} In Fig. 6 the dependence of G/ω on C is presented for the Ni/

ZnO/n-Si heterostructure with a 135-nm-thick ZnO layer. Different curves correspond to gate voltages varying from -0.5 V to 0.5 V with the step of 0.2 V. From these complex impedance plots, the effective carrier lifetime can be estimated, because the highest point of the semicircle in the Cole–Cole plot corresponds to a characteristic carrier recharging frequency, the reciprocal of which is the effective carrier lifetime.³¹

Figure 7 shows time constants derived from Cole–Cole plots for four samples. At positive voltages, the time constant is related mainly to the carrier exchange between the interface traps and the silicon conduction band. This is also confirmed by an exponential drop of the characteristic time with increasing the gate voltage.^{32,33} At negative biases, two different processes can be distinguished. The first one is related

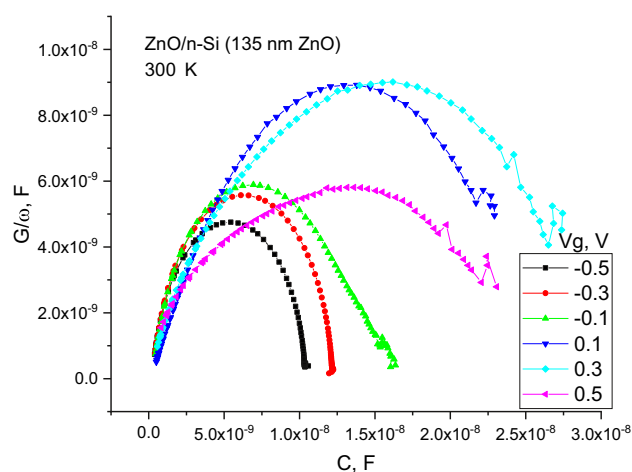


Fig. 6 Cole–Cole plot for the Ni/ZnO/n-Si heterostructure for different gate voltages.

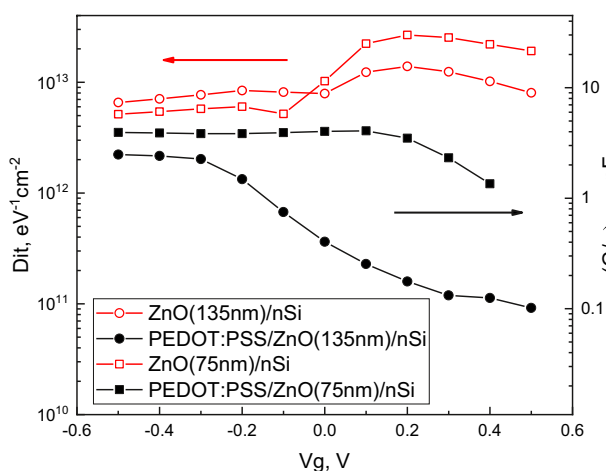


Fig. 5 Dependences of density of interface states on gate voltage for the Ni/ZnO/n-Si heterostructure and the Au/PEDOT:PSS/ZnO/n-Si hybrid heterostructure.

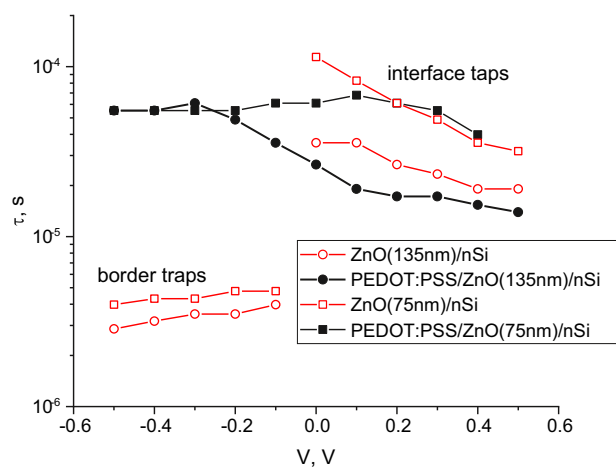


Fig. 7 Time constant, τ , as a function of applied bias for the Ni/ZnO/n-Si heterostructure and the Au/PEDOT:PSS/ZnO/n-Si hybrid heterostructure.

to the interface traps and is observed in all the samples, and the second one, with much shorter characteristic times, is observed in the structures without a PEDOT:PSS layer, and is due to the recharging of the border traps.³² The impedance analysis shows that, after deposition of a PEDOT:PSS layer, these traps become inactive under operational conditions, and the respective fast recharging process is eliminated. This phenomenon is associated with the formation of the inversion layer and with the Fermi level location near the valence band at the ZnO/Si interface, due to the increase of the silicon surface potential barrier. In this case, the characteristic time determined from the Cole–Cole diagram corresponds to the generation time of the minority carriers.

Photoelectrical Properties of n^+ -ZnO/ n -Si and PEDOT:PSS/ n^+ -ZnO/ n -Si Heterostructures.

Table II summarizes the results of electrophysical and photoelectric measurements of the heterostructures. The open-circuit voltage, V_{oc} , and the short-circuit current, I_{sc} , were measured with illumination by a light source simulating the sun's irradiation under AM1.5 conditions. The open-circuit voltage is significantly (by 54–180%) higher in samples with a layer of PEDOT:PSS. This correlates with a higher barrier at the ZnO/Si interface. The value of the open-circuit voltage, V_{oc} , is determined by the stationary value of the excess concentration of non-equilibrium minority current carriers, $\Delta p = \Delta n$ ³⁴:

$$V_{oc} = \frac{nkT}{q} \ln \left(\frac{\Delta p}{p_0} + 1 \right) + \frac{nkT}{q} \ln \left(\frac{\Delta p}{n_0} + 1 \right) \quad (4)$$

where q is the electron charge, k is the Boltzmann constant, p_0 and n_0 are the concentrations of minority and majority charge carriers, respectively, and n is the ideality factor.

For the case of low excitation levels ($\Delta p < n_0$), which is the case in our study, the value of V_{oc} is determined by the first term of Eq. 1, and, since $\Delta p/p_0 > 1$:

$$V_{oc} \approx \frac{nkT}{q} \ln \left(\frac{\Delta p}{p_0} \right) \propto \ln(\Delta p) \quad (5)$$

In turn, the effective lifetime of excess minority carriers is proportional to Δp : $\tau_{eff} \sim \Delta p$.

Thus, a significant increase in the open-circuit voltage indicates a significant increase in the effective lifetime of excess minority carriers in the ZnO/Si samples after the deposition of the PEDOT:PSS layer. Since the effective lifetime is expressed as:

$$\frac{1}{\tau_{eff}} = \frac{1}{\tau_b} + \frac{S_{\Sigma}}{d} \quad (6)$$

where $S_{\Sigma} = S_f + S_b + V_{SCR}$, S_{Σ} is the effective surface recombination rate, which is equal to the sum of the surface recombination rates on the front S_f and back S_b surfaces and the recombination rate, V_{SCR} , in the space charge region (SCR) of the heterojunction, τ_b is the volume lifetime, and d is the sample thickness.

When applying the PEDOT:PSS layer, the volume lifetime, τ_b , does not change; therefore, a significant increase in the effective lifetime indicates a decrease in recombination losses on the frontal surface and the recombination rate in the SCR. Thus, the deposition of a PEDOT:PSS layer on the frontal surface of samples of ZnO/Si heterostructures effectively electrically “passivates” the near-surface region of these structures, due to the strong increase of the surface potential barrier. In Ref. 35, it was shown that the surface recombination rate strongly decreases when the silicon interface is under the strong inversion condition.

Finally, the spectral dependences of the EQE were measured, and the resulting spectra are presented in Fig. 8. The decrease of EQE at a wavelength longer than 600 nm is evidently related to the substantial drop of transmittance in this spectral range after deposition of the PEDOT:PSS layer, which limits the light absorption in the silicon. Visually, it is manifested as the dark-blue, almost black, color of the PEDOT:PSS film deposited onto the ZnO surface, although the same films deposited on silicon or glass are transparent. In Ref. 36, the PEDOT:PSS/ZnO nanocomposites were studied which also had dark-blue and black colors. In Ref. 37, the electrochromic device was proposed by the addition of Fe_2O_3 oxide into the PEDOT:PSS film, and it was shown that, applying the reduction potential changes, the color of the film becomes dark blue, and the oxidation

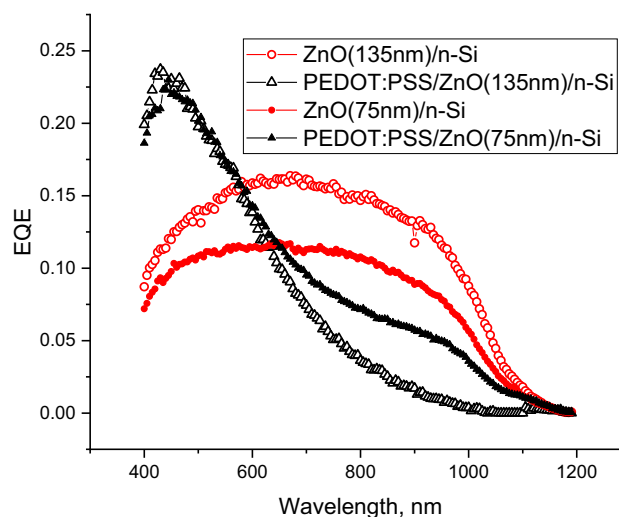


Fig. 8 Spectral dependences of external quantum efficiency (EQE) for the Ni/ZnO/ n -Si heterostructure and the Au/PEDOT:PSS/ZnO/ n -Si hybrid heterostructure.

potential makes the film transparent. The transmittance spectrum for the reduced state of PEDOT:PSS shows a sharp drop in wavelengths in the 550–750 nm range. Therefore, it is reasonable to suggest that, in our case, after the deposition of PEDOT:PSS onto zinc oxide, the PEDOT:PSS film is being reduced, changing its color and causing effective light trapping. The reduction–oxidation reaction is probably in this case due to the high chemical activity of zinc. Another consequence of this reaction is the additional oxidation of ZnO, which can result in a decrease in the concentration of oxygen vacancies, which are often considered as intrinsic electron dopants. This can further increase the layer resistance and suppress the short-circuit current.

The sharp increase of EQE in the short wavelength range after the deposition of PEDOT:PSS can be explained by the effective passivation of the near-surface region of these structures noted above. An additional contribution can be made by carriers generated and spatially separated in the PEDOT:PSS and ZnO layers under illumination, which is confirmed by the increase of V_{OC} after the PEDOT:PSS deposition. ZnO is sensitive to violet and ultraviolet radiation because of its high band gap, but, in the absence of PEDOT:PSS, the generated carriers do not contribute to the total photogenerated current. The potential barrier at the PEDOT:PSS/ZnO interface drives the carriers to the silicon, and the electrically “passivated” interface suppresses surface recombination of the photoexcited carriers. Therefore, the quantum efficiency in the short wavelength range increases.

EQE in the long wavelength range (> 600 nm) mainly originates from the charge carriers generated in the SCR of the silicon substrate, since PEDOT:PSS and ZnO demonstrate weak optical absorption in this spectral range. Therefore, some portion of light can be reflected by the rough PEDOT:PSS layer, causing a slight decrease in the EQE for the PEDOT:PSS/ZnO(75 nm)/*n*-Si sample compared to the reference sample without polymer coverage. Lower values of EQE for the ZnO(75-nm)/*n*-Si sample as compared to the ZnO(135-nm)/*n*-Si sample can be explained by the higher series resistance, R_S , and slightly higher built-in voltage, V_{bi} (see Table II). Additionally, the ideality factor for the structure with the thinner film is higher, reflecting the poor interface quality which results in the higher interface recombination rate.

Conclusions

We have studied the effect of the deposition of the PEDOT:PSS layer on the surface of zinc oxide in ZnO/*n*-Si heterostructures. It was found that deposition of PEDOT:PSS increases the barrier, turning the ZnO/Si interface into strong inversion, which effectively electrically “passivates” the near-surface region. The border traps with a short time

constant are not detected after the deposition. Photoelectric measurements have shown that the addition of the organic layer significantly, by 54–180%, increases the open-circuit voltage, but at the same time reduces the short-circuit current due to the low transmission and high resistance of the PEDOT:PSS film. In the blue range, the EQE increases due to both the effective electrical “passivation” of the near-surface region of these structures and the additional contribution of carriers generated in the PEDOT:PSS and ZnO layers.

Supplementary Information The online version contains supplementary material available at <https://doi.org/10.1007/s11664-023-10276-2>.

Acknowledgments The work was (partially) supported by the Ministry of Education and Science of Ukraine in the frame of the joint research programs of Ukraine and Czech Republic (project #M/22-2022), by the Program Science for Peace and Security (NATO project SPS G5853). The authors are grateful to Dr. P. M. Lytvyn for conducting scanning spreading resistance microscopy measurements.

Conflict of interest Authors declare that they have no conflict of interest.

Open Access This article is licensed under a Creative Commons Attribution 4.0 International License, which permits use, sharing, adaptation, distribution and reproduction in any medium or format, as long as you give appropriate credit to the original author(s) and the source, provide a link to the Creative Commons licence, and indicate if changes were made. The images or other third party material in this article are included in the article's Creative Commons licence, unless indicated otherwise in a credit line to the material. If material is not included in the article's Creative Commons licence and your intended use is not permitted by statutory regulation or exceeds the permitted use, you will need to obtain permission directly from the copyright holder. To view a copy of this licence, visit <http://creativecommons.org/licenses/by/4.0/>.

References

1. J. Ding, Y. Zhou, G. Dong, M. Liu, D. Yu, and F. Liu, Solution-processed ZnO as the efficient passivation and electron selective layer of silicon solar cells. *Prog. Photovolt. Res. Appl.* 26, 974 (2017).
2. R. Romero, M.C. López, D. Leinen, F. Martin, and J.R. Ramos-Barrado, Electrical properties of the *n*-ZnO/*c*-Si heterojunction prepared by chemical spray pyrolysis. *Mater. Sci. Eng. B* 110, 87 (2004).
3. D. Song and B. Guo, Electrical properties and carrier transport mechanisms of *n*-ZnO/SiO_x/*n*-Si isotype heterojunctions with native or thermal oxide interlayers. *J. Phys. D: Appl. Phys.* 42, 025103 (2009).
4. X. Huang, K. Wang, C. Yi, T. Meng, and X. Gong, Efficient perovskite hybrid solar cells by highly electrical conductive PEDOT:PSS hole transport layer. *Adv. Energy Mater.* 6, 1501773 (2016).
5. M.-U. Halbach, D. Zielke, R. Gogolin, R. Sauer, W. Lövenich, and J. Schmidt, Reduction of parasitic absorption in PEDOT:PSS at the rear of *c*-Si solar cells. *AIP Conf. Proc.* 1999, 040008 (2018).
6. D. Zielke, A. Pazidis, F. Werner, and J. Schmidt, Organic-silicon heterojunction solar cells on *n*-type silicon wafers: the BackPEDOT concept. *Sol. Energy Mater. Sol. Cells* 131, 110 (2014).

7. S. Jäckle, M. Liebhaber, C. Gersmann, M. Mews, K. Jäger, S. Christiansen, and K. Lips, Potential of PEDOT:PSS as a hole selective front contact for silicon heterojunction solar cells. *Sci. Rep.* 7, 2170 (2017).
8. Q. Li, J. Yang, S. Chen, J. Zou, W. Xie, and X. Zeng, Highly conductive PEDOT:PSS transparent hole transporting layer with solvent treatment for high performance silicon/organic hybrid solar cells. *Nanoscale Res. Lett.* 12, 506 (2017).
9. M.U. Khan, G. Hassan, M.A. Raza, J. Bae, and N.P. Kobayashi, Schottky diode based resistive switching device based on ZnO/PEDOT:PSS heterojunction to reduce sneak current problem. *J. Mater. Sci. Mater. Electron.* 30, 4607 (2019).
10. E. Frau, Y. Zhang, L. Viau, F. Jurin, C. Buron, C. Filiâtre, and S. Schintke, Inkjet printable ZnO/PEDOT:PSS heterojunction for thin flexible semi-transparent optoelectronic sensors, in *2020 22nd International Conference on Transparent Optical Networks (ICTON)*, 1 (2020)
11. R.D. Ladhe, K.V. Gurav, S.M. Pawar, J.H. Kim, and B.R. Sankapal, p-PEDOT:PSS as a heterojunction partner with n-ZnO for detection of LPG at room temperature. *J. Alloys Compd.* 515, 80–85 (2012).
12. K. Shahi, R.S. Singh, N.P. Singh, M. Aleksandrova, and A.K. Singh, Synthesis and characterization of PEDOT:PSS/ZnO nanowires heterojunction on ITO coated plastic substrate for light-emitting diodes. *Mater. Today: Proc.* 15, 394 (2019).
13. M. Belhaj, C. Dridi, R. Yatskiv, and J. Grym, The improvement of UV photodetection based on polymer/ZnO nanorod heterojunctions. *Org. Electron.* 77, 105545 (2020).
14. R. Yatskiv, J. Grym, S. Tiagul'skiy, and N. Bašinová, Influence of surface polarity on optoelectronic properties of PEDOT:PSS/ZnO hybrid heterojunctions. *Phys. Status Solidi A* 218, 2000612 (2021).
15. A.V. Vasin, A.V. Rusavsky, E.G. Bortchagovsky, Y.V. Gomeniuk, A.S. Nikolenko, V.V. Strelchuk, R. Yatskiv, S. Tiagul'skiy, S. Prucnal, W. Skorupa, and A.N. Nazarov, Methane as a novel doping precursor for deposition of highly conductive ZnO thin films by magnetron sputtering. *Vacuum* 174, 109199 (2020).
16. A.V. Vasin, A.V. Rusavsky, S.V. Mamykin, A.S. Nikolenko, V.V. Strelchuk, R. Yatskiv, J. Grym, A.I. Gudymenko, V.P. Kladko, I.P. Tyagul'skiy, J. Lorinčik, I. Elantsev, and A.N. Nazarov, On the nature of doping effect of methane in ZnO thin films deposited by RF-magnetron sputtering. *J. Mater. Sci.: Mater. Electron.* 33, 6421 (2022).
17. S.M. Sze and K.K. Ng, *Physics of Semiconductor Devices* (New York: Wiley, 2007).
18. E.H. Rhoderick and R.H. Williams, *Metal – Semiconductor Contacts* (Press: Oxford Univ, 1988).
19. J.M. Ghushe, S.M. Giripunje, and S.B. Kondawar, Fabrication of inorganic/organic hybrid heterojunctions of polyaniline composite/blend for the study of diode characteristics. *J. Phys. Sci.* 28, 99 (2017).
20. B.K. Sharma, N. Khare, and S. Ahmad, A ZnO/PEDOT:PSS based inorganic/organic heterojunction. *Solid State Comm.* 149, 771 (2009).
21. J. Rodriguez-Moreno, E. Navarrete-Astorga, F. Martin, R. Schreiber, J.R. Ramos-Barrado, and E.H. Dalchiale, Semitransparent ZnO/poly(3,4-ethylenedioxythiophene) based hybrid inorganic/organic heterojunction thin film diodes prepared by combined radio-frequency magnetron-sputtering and electrodeposition techniques. *Thin Solid Films* 525, 88 (2012).
22. S.K. Cheung and N.W. Cheung, Extraction of Schottky diode parameters from forward current-voltage characteristics. *Appl. Phys. Lett.* 49, 85 (1986).
23. E.H. Nicollian and A. Goetzberger, MOS conductance technique for measuring surface state parameters. *Appl. Phys. Lett.* 7, 216 (1965).
24. E.H. Nicollian and J.R. Brews, *MOS Physics and Technology* (New York: Wiley, 1982).
25. Y. Gomeniuk, A. Nazarov, Y. Vovk, Y. Lu, O. Buiiu, S. Hall, J.K. Efavi, and M.C. Lemme, Low-temperature conductance measurements of surface states in HfO₂-Si structures with different gate materials. *Mater. Sci. Semicond. Process.* 9, 980 (2006).
26. T. Walter, R. Herberholz, C. Müller, and H.W. Schock, Determination of defect distributions from admittance measurements and application to Cu(In, Ga)Se₂ based heterojunctions. *J. Appl. Phys.* 80, 4411 (1996).
27. S. Monaghan, E. O'Connor, R. Rios, F. Ferdousi, L. Floyd, E. Ryan, K. Cherkaoui, I.M. Powey, K.J. Kuhn, and P.K. Hurley, Capacitance and conduction for an MOS system in inversion, with oxide capacitance and minority carrier lifetime extractions. *IEEE Trans. Electron Devices* 61, 4176 (2014).
28. P.C. Malmin, Cole-cole plotting of surface state admittance in MIS capacitors. *Phys. Status Solidi A* 8, 597 (1971).
29. G. Garcia-Belmonte, P.P. Boix, J. Bisquert, M. Sessolo, and H.J. Bolink, Simultaneous determination of carrier lifetime and electron density-of-states in P3HT:PCBM organic solar cells under illumination by impedance spectroscopy. *Sol. Energy Mater. Sol. Cells* 94, 366 (2010).
30. A. Kaphle, E. Echeverria, D.N. McIlroy, and P. Hari, Enhancement in the performance of nanostructured CuO-ZnO solar cells by band alignment. *RSC Adv.* 10, 7839 (2020).
31. S. Kumar, Vandana, C.M.S. Rauthan, V.K. Kaul, S.N. Singh, and P.K. Singh, Spectral and injection level dependence of recombination lifetimes in silicon measured by impedance spectroscopy. *IEEE J. Photovolt.* 4, 380 (2014).
32. H. Kim, S. Choi, and B.J. Choi, Influence of AlN and GaN pulse ratios in thermal atomic layer deposited AlGaIn on the electrical properties of AlGaIn/GaN Schottky diodes. *Coatings* 10, 489 (2020).
33. P. Kordoš, R. Stoklas, D. Gregušová, and J. Novák, Characterization of AlGaIn/GaN metal-oxide-semiconductor field-effect transistors by frequency dependent conductance analysis. *Appl. Phys. Lett.* 94, 223512 (2009).
34. A.V. Sachenko, A.I. Skrebtii, R.M. Korkishko, V.P. Kostilyov, N.R. Kulish, and I.O. Sokolov'skiy, Simulation of the real efficiencies of high-efficiency silicon solar cells. *Semiconductors* 50, 523 (2016).
35. A.P. Gorban, V.P. Kostilyov, A.V. Sachenko, A.A. Serba, and I.O. Sokolov'skiy, Impact of excess charge carrier concentration on effective surface recombination velocity in silicon photovoltaic structures. *Ukr. J. Phys.* 51, 598 (2006).
36. W. Lee, S. Lee, H. Kim, and Y. Kim, Organic thermoelectric devices with PEDOT:PSS/ZnO hybrid composite. *Chem. Eng. J.* 415, 128935 (2021).
37. D. Lévassieur, I. Mjejri, T. Rolland, and A. Rougier, Color tuning by oxide addition in PEDOT:PSS-based electrochromic devices. *Polymers* 11, 179 (2019).

Publisher's Note Springer Nature remains neutral with regard to jurisdictional claims in published maps and institutional affiliations.